

03,04,08

Ab initio calculations of electronic properties and charge transfer in $Zn_{1-x}Cu_xO$ with wurtzite structure

© M.M. Asadov^{1,2}, S.N. Mustafaeva³, S.S. Guseinova³, V.F. Lukichev⁴

¹ Institute of Catalysis and Inorganic Chemistry named after Academician M. Nagiyev, Azerbaijan National Academy of Sciences,

Baku, Azerbaijan

² Scientific research institute of Geotechnological Problems of Oil, Gas and Chemistry, ASUOI,

Baku, Azerbaijan

³ Institute of Physics, National Academy of Sciences of Azerbaijan,

Baku, Azerbaijan

⁴ Valiev Institute of Physics and Technology, Russian Academy of Sciences,

Moscow, Russia

E-mail: mirasadov@gmail.com

Received January 7, 2022

Revised January 7, 2022

Accepted January 8, 2022

The results of studying the electronic structure and the influence of the local environment of the copper impurity on the properties and magnetic moment in supercells in $Zn_{1-x}Cu_xO$ are presented. DFT calculations were carried out in the local electron density (LDA) and generalized gradient approximation (GGA). The band structure of in $Zn_{1-x}Cu_xO$ was calculated taking into account the correction for spin polarization and the strong electronic interaction. DFT LSDA + U and SGGA + U (U is the Coulomb interaction) calculations made it possible to take into account the contributions of the $3d$ shells of the Zn and Cu cations to the band spectrum of in $Zn_{1-x}Cu_xO$. The introduction of copper into the ZnO lattice leads to a change in the impurity and valence bands of in $Zn_{1-x}Cu_xO$. In this case, the bottom of the in $Zn_{1-x}Cu_xO$ conduction band shifts towards low energies. The total density of electronic states of in $Zn_{1-x}Cu_xO$ near the Fermi level is mainly determined by the $3d$ states of Zn and Cu and the $2p$ state of oxygen. ZnO doped with copper acquires a magnetic moment.

The introduction of a vacancy into a supercell in $Zn_{1-x}Cu_xO$ noticeably changes the local magnetic moment. As the copper concentration in $Zn_{1-x}Cu_xO$ ($x = 0, 0.01, \text{ and } 0.02$) increases, the conductivity of the samples in both constant and alternating current increased, and the activation energy of conduction decreased.

Keywords: ZnO, copper doping, density functional theory, band calculations, electronic structure, localized magnetic moment, defect formation energies, $Zn_{1-x}Cu_xO$, charge transfer, parameters of localized states.

DOI: 10.21883/PSS.2022.05.54011.270

1. Introduction

The active structural materials of electronic and optoelectronic devices are based on the manufacture of n - and p -type doped semiconductors. Such materials include doped zinc oxide (ZnO) used, for example, for voltage-variable resistors (VVRs). ZnO-based voltage-variable resistors can protect circuits in a wide voltage range from several volts up to 1000 kV AC (for low-voltage VVRs) and 1100 kV DC in power transmission and distribution systems [1]. Composition, structure and property control knowledge is necessary to control the material doping process. *Ab initio* calculations make an important contribution to this knowledge.

In addition, a wide and straight band gap ($E_g \approx 3.37$ eV) and high exciton bond energy (~ 60 meV), high electron mobility and high thermal conductivity make n -type conductivity ZnO suitable for a wide range of devices [2].

ZnO-based materials are promising for the development of thin film transistors, photodetectors, UV-, blue, green and white LEDs. ZnO-based nanomaterials are used in various

technology areas, in particular, in sensor, capacitor, solar cell, ultraviolet laser, generator and optoelectronic device design [3].

For doping of ZnO, as with other semiconductors, take into account the structural features of ZnO. According to various authors, a ZnO lattice cell with a hexagonal crystal system has the following parameters: $a = 3.2475\text{--}3.2501$ Å (in the basal plane) and $c = 5.2042\text{--}5.2075$ Å (in the basal direction). The ZnO structure consists of two interpenetrating hexagonally-packed sublattices. Each sublattice includes four atoms per an elementary cell. Each zinc atom is surrounded with four oxygen atoms that are located in the tetrahedron angles and four zinc atoms surround each oxygen atom, respectively. The material properties depend on its crystal-lattice orientation. ZnO contains various types of intrinsic defects with various ionization energies. Interstitial zinc and oxygen vacancies are the prevailing types of ion defects in undoped ZnO.

Group I elements are used as substituting acceptor impurities for ZnO. They create shallow energy levels.

Group I elements can also occupy interstitial positions. If $E_F = E_{VB}$ (where E_F is Fermi energy, E_{VB} — is the valance band energy), then incorporation into interstices is preferable, for example, for Li and Na [4].

Cu incorporation into ZnO compounds causes specific effects. Copper as an acceptor defect introduces various local levels into the ZnO band gap. Therefore, the study of $Zn_{1-x}Cu_xO$ structure and properties is a priority task [5–7]. Copper subgroup elements (Cu, Ag and Au) are included in a secondary subgroup of group I. Their atoms have one s -electron on their external level with additional d -electrons on the pre-external level of these atoms besides s - and p -electrons. Due to d -electrons in the compounds, copper subgroup elements show both oxidation number 1+ and high oxidation numbers (in particular, Cu^{2+}).

$Zn_{1-x}Cu_xO$ materials are produced using both hydrothermal synthesis [8] and solid-state reaction method [9]. Properties of one-dimensional materials produced from pure ZnO and copper-doped ZnO investigated in the same conditions are described in [8]. Low-dimensional sensors based on ZnO–Cu have higher sensitivity at room temperature, lower response time and selectivity. Such sensors are offered for H_2 detection with low power consumption.

The copper-doped ZnO nanopowder properties are influenced by annealing effects, temperature and Cu dopant concentration [9]. The X-ray diffraction has shown that Cu ions successfully substitute Zn ions in a hexagonal of wurtzite in ZnO. The band gap is reduced as a result of Cu incorporation in the ZnO structure. Cu doping also alters the magnetic properties of ZnO nanopowders. Ferromagnetic behavior of ZnO nanopowders is reduced with higher Cu concentration. Oxygen stoichiometry (oxygen vacancies) in ZnO nanopowders also influences the ferromagnetic response at room temperature.

The experimentally studied $T-x$ phase diagram of the ZnO– Cu_2O quasi-binary system shows no solid solubility. This is due to the fact that dimensions and chemical properties of the interacting components are very different [10]. ZnO– Cu_2O is an eutectic system with an eutectic point at $T = 1299$ K and $x = 0.126$ mol.% ZnO. In this system, the restricted solid solubility based on ZnO and Cu_2O is probably $\sim 1-2$ mol.%. No solubility of Cu_2O in the ZnO matrix at the eutectic point from $T-x$ diagram (at $P(O_2) = 0.21$ atm) is detected either. To achieve the high concentration of free carriers in $Zn_{1-x}Cu_xO$, high concentration of Cu dopant shall be obtained. The maximum concentration that can be achieved by Cu dopant in the ZnO semiconductor in thermodynamic equilibrium conditions corresponds to Cu solubility in Cu–ZnO system. $T-x$ diagram Cu_2O –ZnO [10] shows that Cu solubility in ZnO is negligible in a wide temperature range. Therefore the doping control issue and investigation of composition–structure–properties relationship in ZnO–Cu are essential.

The degree of solubility of acceptor impurities, for example, (Na, Li and N) restricts the hole concentration in ZnSe

and ZnTe compounds equivalent to ZnO [11]. Therefore, the investigation of patterns of copper influence on the electronic structure [12], dielectric [13], optical [14,15], magnetic [16–18] and other physical properties [19] of the materials based on n - and p -type ZnO is also a challenging problem. In view of possible production of minidevices, doped ZnO nanocrystalline powders and thin films are also addressed [20].

Electronic structure, density of states and optical absorption properties of copper-doped ZnO have been studied, for example, in [12] using *ab initio* method. For initial $Zn_{1-x}Cu_xO$ ($x = 0, 0.0278, 0.0417$) structure, geometric optimization and energy calculation have been carried out and compared with the experimental findings. It has been shown that $Zn_{1-x}Cu_xO$ band gap is reduced with an increase in Cu concentration. Zinc substitution in ZnO with Cu atom results in red shift of the optical absorption edge which is in agreement with the experimental results.

And [13] shows that the dielectric constants and dielectric losses in $Zn_{1-x}Cu_xO$ nanocomposites decrease with an increase in Cu concentration in ZnO. However, conductivity grows with an increase in x and superimposed alternating field frequency. Direct current conductivity in $Zn_{1-x}Cu_xO$ is also increased as a result of the increase in Cu concentration and temperature. Authors of [13] were limited only to listing of the findings without any explanations and did not explore the conduction mechanism in $Zn_{1-x}Cu_xO$. In addition, the given concentration of Cu dopant is higher than the possible Cu solubility limit in ZnO.

The problem of copper-doped p -type ZnO production may be attributed to self-compensation of intrinsic point defects. Effective ionic radii of Cu^{2+} and Zn^{2+} are close to each other. This is also important for concentration control of impurities and intrinsic defects in ZnO in order to obtain materials with specified n - or p -type conductivity. Every attempt to incorporate Cu doping acceptor atoms into ZnO lattice will be accompanied with a spontaneous generation of defects, for example, oxygen and zinc vacancies. These defects may serve as donors for Cu acceptor. Therefore, such acceptor compensation with vacancies shall restrict the doping level of ZnO. In addition, in $Zn_{1-x}Cu_xO$ anisotropic $3d$ electron clouds of zinc and copper ions may be exposed to the electrostatic field created by the surrounding ions. As a result, the system energy may be different when magnetic moments are oriented along different crystal directions which may cause magnetic anisotropy in $Zn_{1-x}Cu_xO$. Ferromagnetic alignment capability is defined by the Fermi-level density of electronic states and exchange interaction in the system. Taking into account the density functional theory within the band model, the magnetic moment variation in materials may be explained. However, the above effects in $Zn_{1-x}Cu_xO$ have been understudied, both theoretically and experimentally.

In view of the above problems, features of the electronic structure, localized and band states of electrons and semiconductor structure magnetism based on a copper-doped

ZnO compound have been studied herein. The purpose of the study included *ab initio* calculation of the magnetic properties of $Zn_{1-x}Cu_xO$ super cells (wurtzite structure), investigation of the electrical and dielectric properties of the prepared samples ($x = 0.01$ and 0.02) and the study of the charge transfer parameters with a change in copper concentration in the system.

2. Calculation technique and experiment

2.1. Calculation model and details

The geometry, electronic structure and magnetic moment of the impurity centers were calculated using the *ab initio* method. The studied hexagonal structure models of ZnO-based wurtzite comprised $Zn_{1-x}Cu_xO$ polyatomic super cells where Cu atom substitutes Zn atom. In particular, $Zn_{0.875}Cu_{0.125}O$ ($2 \times 2 \times 1$) and $Zn_{0.944}Cu_{0.056}O$ ($3 \times 3 \times 1$) super cells with Cu atom that substitutes Zn atom were studied. The calculations were based on the electron density functional theory (DFT) using Atomistix Tool Kit. exchange-correlation interaction was studied in the local density approximations (LDA) taking into account the local spin density approximation (LSDA) and by the generalized gradient approximation (GGA) method using the Perdew–Burke–Ernzerhof (PBE) functional [21,22]. The plane wave cutting energy in the pseudo-wave function calculation was equal to 30 Ry. The charge density cutting energy was equal to 300 Ry. Zn $3d^{10}4s^2$, Cu $3d^{10}4s^1$ and O $2s^22p^4$, respectively, were used as the valence electronic configurations. The DFT calculations of $Zn_{1-x}Cu_xO$ super cell energy were carried out by means of numerical integration by generation of k -points in a Brillouin zone using the Monkhorst–Pack method with a plane grid constructed with a (0.5, 0.5, 0.5) shift from the origin of coordinates. Relaxation of the lattice parameters and $Zn_{1-x}Cu_xO$ crystal atom positions was carried out until the forces acting between the atoms became less than $0.5 \text{ meV}/\text{\AA}$. In this case, the maximum mechanical stress tensor was $\leq 0.1 \text{ meV}/\text{\AA}^3$. Optimization of $Zn_{1-x}Cu_xO$ structure was continued until the structural parameter equilibrium was achieved. The maximum kinetic energy during the wave function separation did not exceed 150 Ry, which ensures good convergence with the total energy of ZnO. Minimization of the total structure energy with an accuracy of $2 \cdot 10^{-5} \text{ eV/atom}$ corresponded to the equilibrium lattice parameter values. While the force applied to each atom was lower than 0.05 eV/nm , tolerance deviation was 0.0002 nm and stress tolerance was 0.1 GPa . The DFT calculations included the contributions of the spin-orbit interaction of Zn and Cu d -electrons and localized oxygen p -electrons in $Zn_{1-x}Cu_xO$. In order to enhance the magnetic state of acceptor copper, zinc vacancies were added to the structure at a maximum distance from the impurity atom. To improve the accuracy, a term allowing for the electron-electron correlations (U is a Coulomb interaction parameter) between the atoms ($U = 5 \text{ eV}$ is the

repulsion energy) which is described by the Hubbard model [23] was introduced in the LSDA and SGGA calculations.

2.2. Preparation of samples

The $Zn_{1-x}Cu_xO$ ($x = 0.01$ and 0.02) compound samples were synthesized by the solid-state reaction method with thorough mixing of ZnO (99.99%) and Cu_2O (99.99%) powders. Stoichiometric amounts of ZnO and Cu_2O were comminuted and then the powder was ignited in air at 1200°C during 12 h followed by furnace cooling down to room temperature. The obtained material was compacted and baked at 500°C in air during 11 h followed by furnace cooling. For homogenization, the samples were annealed at 600°C during 8 h in air. The structural properties of the samples were determined by the X-ray diffraction method (XRD, Bruker D2 PHASER) using Cu K_α -radiation ($\lambda = 1.5406 \text{ \AA}$). The prepared ZnO-based samples had a hexagonal crystal system of wurtzite. Dielectric properties of the samples were measured by a resonance technique using a Q meter [24].

3. Results and discussion

3.1. Results of *ab initio* calculations

It is known that zinc oxide crystallizes in three structures.

1. Wurtzite structure, structural type B4, $P6_3mc$ space group, coordination numbers (CN): $CN_{Zn} = CN_O = 4$ (tetrahedral environment);
2. Zinc blend structure, structural type B3, $F\bar{4}3m$ space group, $CN_{Zn} = CN_O = 4$ (tetrahedral environment);
3. Rock salt structure, structural type B1, $Fm\bar{3}m$ space group, $CN_{Zn} = CN_O = 6$ (tetrahedral environment);

ZnO wurtzite crystalline structure belongs to a hexagonal crystal system. In ZnO structure, each zinc ion is surrounded with four oxygen ions with formation of $[ZnO_4]$ structural unit. $a = 0.3249 \text{ nm}$, $c = 0.5205 \text{ nm}$, $\alpha = \beta = 90^\circ$, $\gamma = 120^\circ$ were assumed as the initial parameters of ZnO lattice cell.

$Zn_{1-x}Cu_xO$ lattice structure. After optimization of $Zn_{1-x}Cu_xO$ wurtzite crystalline structure taking into account the equilibrium atomic state, lattice structure parameters were optimized. The band structure, density of states in k -points in the Brillouin zone (Fig. 1, *a*) and $Zn_{1-x}Cu_xO$ band gap were also calculated.

Various types of defects may exist in ZnO structure (Fig. 1, *b*): ionized oxygen vacancies V_O^\bullet , interstitial zinc Zn_i^\bullet , surface oxygen vacancies $V_{O,surf}^\bullet$, free electrons e' , electrons localized near the excess zinc defects, oxygen defects, surface and three-dimensional donors linked with electrons.

In addition to the intrinsic defects, for example, ionized oxygen vacancies V_O^\bullet and interstitial zinc Zn_i^\bullet , ZnO may also have a set of defects, including but not limited to Zn_i , O_{Zn} , V_O [25,26].

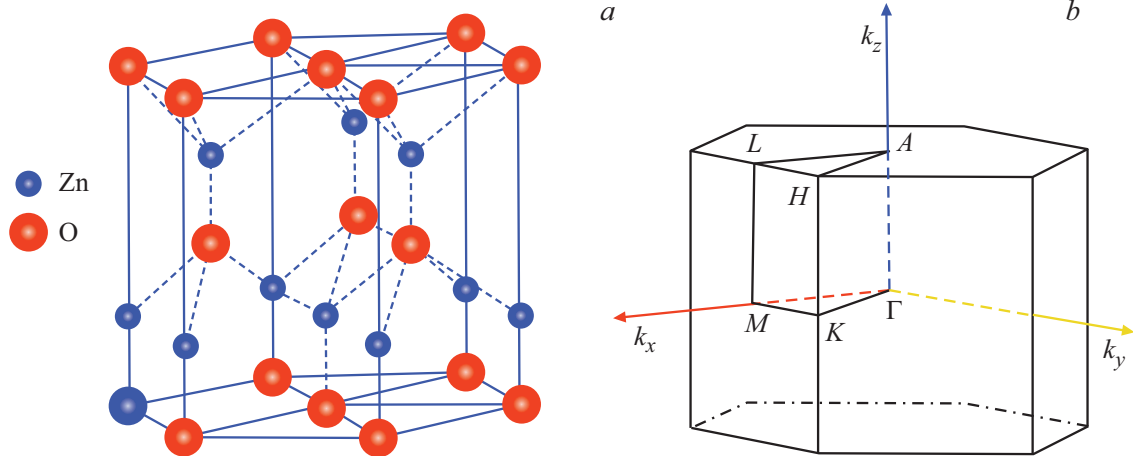


Figure 1. Crystalline structure of ZnO (a) wurtzite and the first Brillouin zone of the hexagonal crystal system (b).

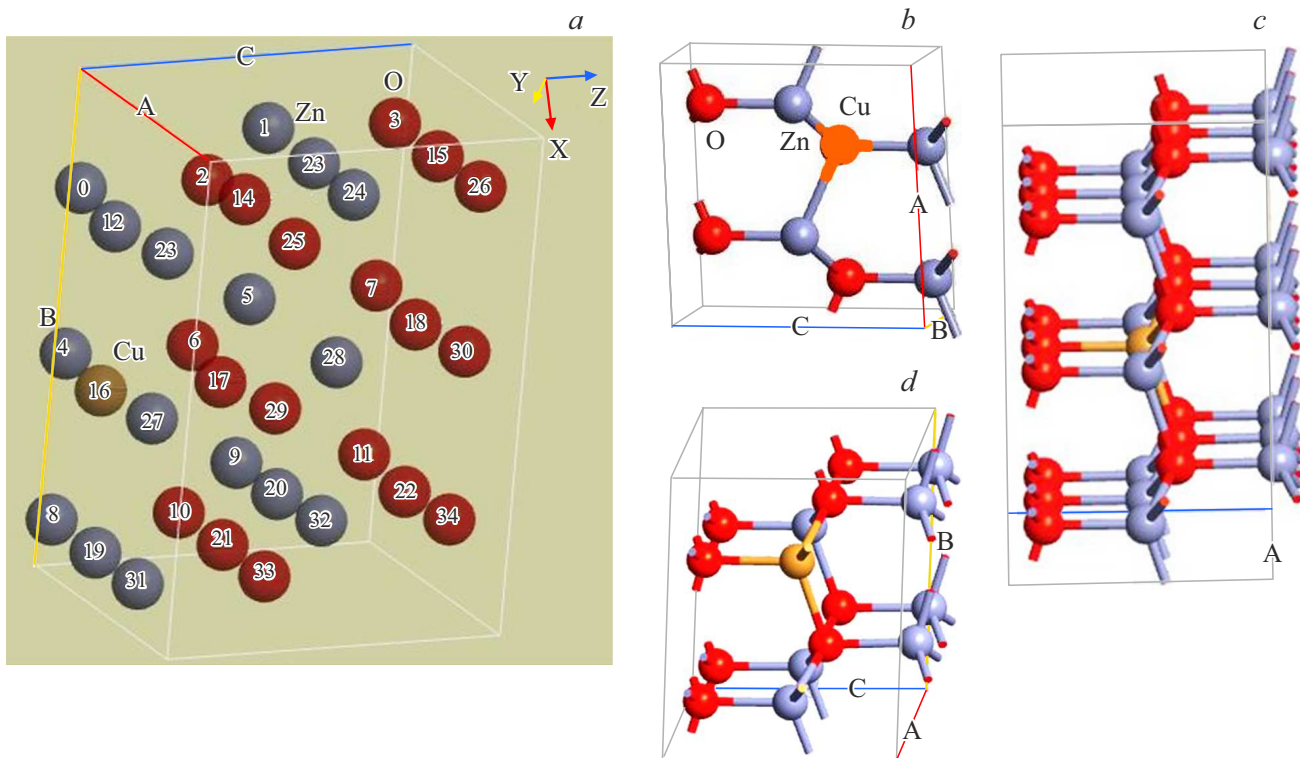


Figure 2. Structures used for wurtzite super cell optimization $Zn_{1-x}Cu_xO$ (a), b — $Zn_{0.99}Cu_{0.01}O$; c — $Zn_{0.944}Cu_{0.056}O$; d — $Zn_{0.875}Cu_{0.125}O$.

Let us denote a copper atom in the zinc sublattice point with Cu_{Zn} . This corresponds to Cu_{Zn}^0 symbol which denotes a copper atom that substitutes zinc and is neutral to ZnO lattice. Within the ion model, Cu_{Zn}^0 may be denoted as $(3d^9) Cu_{Zn}^{2+}$.

According to the known Cu^{2+} (0.057 nm) and Zn^{2+} (0.06 nm) ion radii, it can be believed that the formation of Cu_{Zn} acceptor defects in the zinc sublattice is predominant in the tetrahedral environment of $Zn_{1-x}Cu_xO$ structure. Since copper is in divalent state

and Cu^{2+} and Zn^{2+} ion radii are close to each other in $Zn_{1-x}Cu_xO$, $Zn_{1-x}Cu_xO$ lattice parameters change insignificantly during copper doping. ZnO lattice cell parameters after Cu doping are as follows: $a = 0.32498$ nm, $c = 0.52066$ nm, which complies to the known data (JCPDS card № 00-001-1136).

Optimization of $Zn_{1-x}Cu_xO$ geometrical structure showed that the copper doping influence does not disturb the stability of ZnO hexagonal structure (Fig. 2, a, b, c, d). The optimized parameters of $Zn_{0.944}Cu_{0.056}O$ ($3 \times 3 \times 1$)

Table 1. Comparison of the calculated DFT values for $\text{Zn}_{1-x}\text{Cu}_x\text{O}$ super cell band gap with the optical data

Compound	Calculation, $U_{\text{Cu}3d} = 5 \text{ eV}$	Experiment
	$E_g, \text{ eV}$	
$\text{Zn}_{0.944}\text{Cu}_{0.056}\text{O}$	3.11	3.18 [15]
$\text{Zn}_{0.98}\text{Cu}_{0.02}\text{O}$		

lattice were $a = 0.3247 \text{ nm}$ and $c = 0.5202 \text{ nm}$ and complied with the experimental data.

3.2. $\text{Zn}_{1-x}\text{Cu}_x\text{O}$ band structure

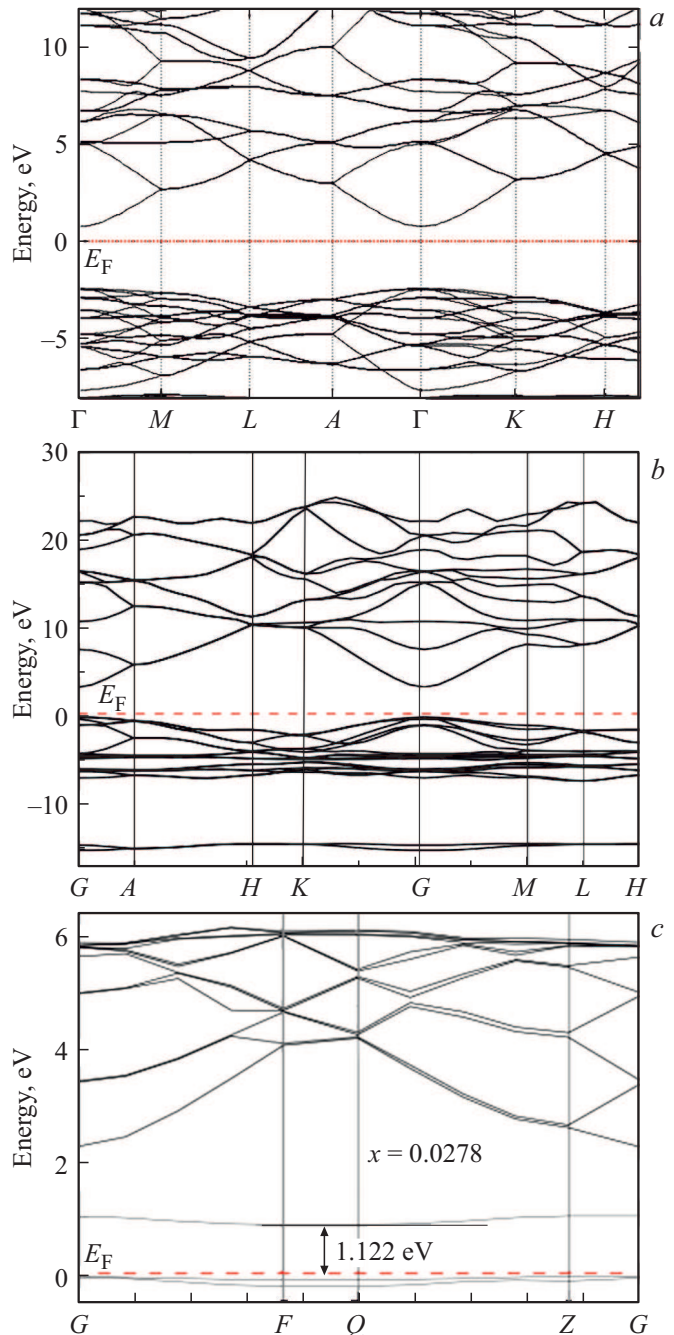
The DFT calculations show that the valence band vertices for the studied ZnO-based super cells are in the Brillouin zone center (point Γ), and the conduction band (CB) minima are in the CB center (Fig. 1, *a*). In other words, the studied $\text{Zn}_{1-x}\text{Cu}_x\text{O}$ semi-conductor super cells had direct band gaps.

Using the LDA and GGA methods both in pure ZnO and $\text{Zn}_{1-x}\text{Cu}_x\text{O}$ for the band gap width, we have obtained conservative values for E_g . For example, for $\text{Zn}_{0.999}\text{Cu}_{0.001}\text{O}$, E_g calculated by LDA and GGA methods were equal to 0.740 and 0.962 eV, respectively (Fig. 3, *a, b*). For other super cell compositions, conservative values for E_g have been also obtained. In particular, according to the GGA + U calculations for $\text{Zn}_{0.9722}\text{Cu}_{0.0278}\text{O}$ [12], $E_g = 1.122 \text{ eV}$ (Fig. 3, *c*).

In our DFT calculations, for example, the assumed repulsion energy $U_{\text{eff}} = 5 \text{ eV}$ for Zn $5d$, Cu $3d$ and $U_{\text{eff}} = 8 \text{ eV}$ for O $4p$ $\text{Zn}_{0.944}\text{Cu}_{0.056}\text{O}$ ($3 \times 3 \times 1$) give $E_g = 3.11 \text{ eV}$ which is close to the experimental value. The close optical band gap of 3.18 eV for ZnO thin films doped with 2 at.% Cu has been obtained experimentally [15] (Table 1). For pure ZnO, the calculated value for E_g in point Γ is equal to 3.221 eV, which also complies with GGA + U calculation values 3.373 eV [12].

The review of DFT calculations of the energy band distribution and density of states (DOS) of $\text{Zn}_{1-x}\text{Cu}_x\text{O}$ system allows to make the following conclusion. In $\text{Zn}_{1-x}\text{Cu}_x\text{O}$ band structure, the conduction band generally consists of Zn $4s$ and O $2s$ states. However, the valence band consists of Zn $3d$ - and O $2p$ -states, and the bottom of conduction band and top of valence band are defined by Zn $4s$ and O $2p$ states, respectively.

ZnO band gap after Cu doping is reduced. With an increase in the mole fraction of Cu dopant atom ($x = 0, 0.056, 0.125$), $\text{Zn}_{1-x}\text{Cu}_x\text{O}$ band gap is further reduced accordingly. For $\text{Zn}_{1-x}\text{Cu}_x\text{O}$, for example, at $x = 0$; $E_g = 3.221 \text{ eV}$, and at $x = 0.056$; $E_g = 1.027 \text{ eV}$. A similar reduction of E_g with the increase in x with other copper concentrations in $\text{Zn}_{1-x}\text{Cu}_x\text{O}$ has been also found in [12]: at $x = 0$; $E_g = 3.373 \text{ eV}$; $x = 0.0278$; $E_g = 1.122 \text{ eV}$; $x = 0.0417$; $E_g = 1.031 \text{ eV}$.

**Figure 3.** Calculated $\text{Zn}_{0.99}\text{Cu}_{0.01}\text{O}$ (*a* — GGA method) and $\text{Zn}_{0.9722}\text{Cu}_{0.0278}\text{O}$ (*b, c* — GGA + U method) band structures. Fermi level (E_F) at zero.

3.3. Densities of states in $\text{Zn}_{1-x}\text{Cu}_x\text{O}$

The review of the partial densities of states (PDOS) and total density of state (DOS) of $\text{Zn}_{1-x}\text{Cu}_x\text{O}$ (Fig. 4, *a, b, c, d*) allows to make the following conclusion. In $\text{Zn}_{1-x}\text{Cu}_x\text{O}$ conduction band (CB), when zinc is substituted with copper, the conduction band energy E_c mainly depends on the electron energy of Cu $3d$ ($\sim 5.5 \text{ eV}$), O $2p$ ($\sim 1.5 \text{ eV}$) and Cu $3p$ -states. I.e. these electronic states

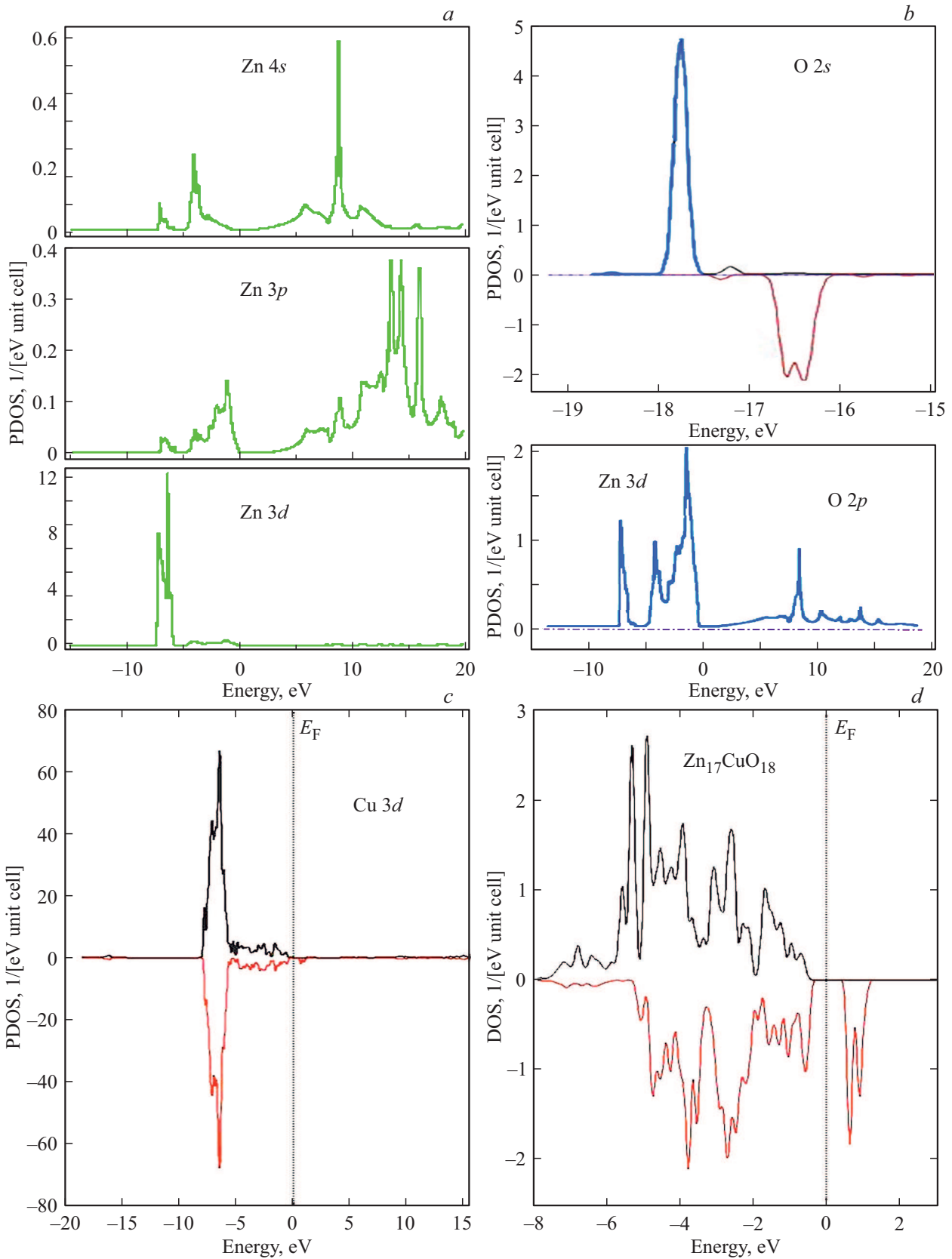


Figure 4. Partial densities of states (PDOS) of s -, p - and d -electrons per atom (a, b, c) and total density of states (DOS) (d) in $Zn_{17}CuO_{18}$ wurtzite super cell calculated by the LSDA + U method, where Zn 4s, 4p, 3d, O 2s, O 2p, Cu 3d lines are shown.

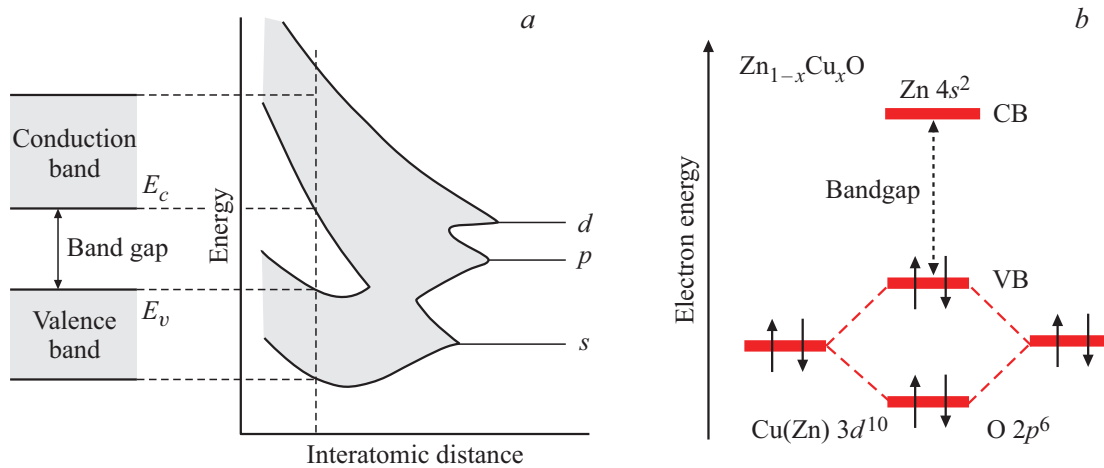


Figure 5. Schematic band diagram of $Zn_{1-x}Cu_xO$ (a) taking into account the hybridization of O $2p$ electrons with Zn(Cu) $3d$ electrons (b).

define the nature of chemical bond in $Zn_{1-x}Cu_xO$ due to the modification of atom valence shells. Thus, the calculations have shown that the total density of electronic states in $Zn_{1-x}Cu_xO$ near the Fermi level is mainly defined by $3d$ -states of Zn and Cu as well as by $2p$ -state of oxygen; contributions associated with s -states of Zn, Cu and O have a significantly lower value.

Within the electron pair repulsion model, Cu $3d$ - and p -electrons of the oxygen and copper components may be assumed as having a repulsion effect due to pd -hybridization. Then, such effect shall cause increase of E_c from the bottom of conduction band and therefore energy E_v is reduced at the top of valence band (VB) (Fig. 5). The specified energy changes in $Zn_{1-x}Cu_xO$ after Cu doping are shown in Fig. 5, a, b.

As has been mentioned before, $Zn_{1-x}Cu_xO$ band gap increases with a decrease in x due to the increase in the energy of the bottom of conduction band. With the increase in Cu concentration in the valence band due to the increase in Cu $3d$ and Cu $3p$ -electrons, respectively, Zn $3d$ -electron concentration is possible reduced. In addition, the electron pair repulsion effect on hybrid pd atomic orbitals. Hybridization may reduce the influence of Zn(Cu) pd -state on the top of valence band. Due to the reduction in Cu concentration, the degree of hybridization of Zn(Cu) d -levels and oxygen p -levels is also reduced. This influences the band structure configuration which, in turn, may cause a change in cation mobility.

On the other hand, with the increase in copper concentration in $Zn_{1-x}Cu_xO$, Cu $3d$ and Cu $3p$ -electron concentration increases and O $2p$ concentration remain unchanged. This results in the increased repulsion effect of p - d -state on the top of valence band. $Zn_{1-x}Cu_xO$ band gap is also reduced accordingly. The valence band moves upwards and the bottom of conduction band moves downwards. Therefore, $Zn_{1-x}Cu_xO$ band gap is reduced with the increase in Cu concentration.

The following conclusion may be made from the foregoing: $Zn_{1-x}Cu_xO$ conduction band is mainly composed of zinc $4s$ -state and oxygen $2s$ -state. Taking into account that the number of copper valence electrons per unit is lower than that of zinc atoms, holes are introduced into the valence band during Cu doping. Whereby the valence band mainly possibly consists of Zn $3d$ and Cu $3d$ states as well as of $2p$ -hybrid state of oxygen. The latter takes place on the top of valence band due to $2p$ -orbital interaction between s - and p -oxygen states, thus $Zn_{1-x}Cu_xO$ band gap is reduced as compared with ZnO. Cu doping causes density localization near the Fermi level in ZnO and in the surrounding Zn orbitals of $2p$ oxygen. While the bottom of $Zn_{1-x}Cu_xO$ conduction band is defined mainly by zinc $4s$ -state that remains unchanged during Cu doping. Thus, the calculations of band structures and densities of electronic states made it possible to interpret the nature of the interband state variation near the structural features in the conduction energy spectrum.

3.4. Defect formation energy

Defect concentration. As a result of thermal fluctuations, heat interchange between the crystal and environment takes place. This causes formation of vacancies and interstitial atoms in the crystal. In the real crystal, thermal defect formation at temperatures other than 0 K reduces the crystal energy. This thermodynamic process occurs as a result of increased S entropy. There is always an equilibrium number of point defects in a crystal. These zero-dimensional defects cause a crystal structure distortion.

In $Zn_{1+x}O$ -based materials, the point defects may appear as intrinsic crystal defects (V_O and V_{Zn} vacancies, O_i and Zn_i interstitial atoms and defect clusters from the matrix atoms) or as impurity defects (substitutional and interstitial impurities as well as impurity clusters). For example, interstitial zinc may be formed according to the following reactions: $O \leftrightarrow 1/2O_2 + Zn_i^{2+} + 2e^-$; $Zn_{Zn} \leftrightarrow Zn_i^0 + V_{Zn}^0$.

The fact that the oxygen vacancies are donor-type centers $O \leftrightarrow 1/2O_2 + V_O^{2-} + 2e^-$; $O \leftrightarrow V_{Zn}^0 + V_O^0$ is one of the causes of the difficulty with the achievement of p -type conduction for ZnO. I.e. V_O^0 vacancies are donors and compensate for acceptor-type impurity defects during ZnO doping. The acceptor-type impurity defects in ZnO have high formation and ionization energies as compared with donor defects.

During generation of point defects, the system consumes some energy, a so called point defect formation energy E_j^f , where, for example, $j = v$ is a vacancy, $j = i$ is an interstitial atom. Energy E_j^f characterizes the energy differences in a crystal containing N -lattice points and one point defect: $E_j^f = E_j - E_0$, where E_j is the crystal energy from N -points with a defect, E_0 is a defect-free crystal energy from N -points. E_j^f is both calculated and defined from the experimental data.

In the thermodynamic equilibrium condition, Gibbs free energy G of the crystal is at its minimum at the specified temperature T and pressure P . Let's consider a crystal volume unit $V = 1 \text{ cm}^3$ that contains N -atoms. Provided that T , P and V are constant, Gibbs free energy is as follows: $G = H - TS$, where H is the crystal enthalpy.

Let's assume that n points are vacant in the crystal volume unit, i.e. $n \ll N$, where n is the numbers of formed defects, N is the number of regular points with atoms participating in the defect formation. Then the free energy minimum G by the number of defects is defined from the crystal equilibrium condition: $\frac{\partial G(n)}{\partial n} = 0$.

The vacancies may be placed in N -points of the crystal by various methods. This will contribute to the configurational entropy S_{conf} during defect formation. Then S_{conf} is defined by the distribution probability W of n vacancies over N -points, i.e. by the number of methods of such vacancy distribution: $S_{\text{conf}} = k_B \ln W$, where k_B is the Boltzmann's constant, $W = \frac{N!}{n!(N-n)!}$ is the number of defect placement options. Using the Stirling formula, at high N we have: $\ln N! \approx N \ln N - N$. Thus, in view of this, we can write the following for S_{conf}

$$S_{\text{conf}} \approx k_B [N \ln N - n \ln n - (N - n) \ln(N - n)]. \quad (1)$$

When there are very few defects in the crystal and they do not interact with each other, then the crystal enthalpy at absolute zero will be equal to the point defect formation energy, for example, for vacancy: $H = nE_v^f$.

In view of the entropy and enthalpy expressions, the Gibbs free energy equation for the crystal is as follows

$$G = nE_v^f - TS_{\text{conf}} \approx nE_v^f - k_B T [N \ln N - n \ln n - (N - n) \ln(N - n)], \quad (2a)$$

$$G = nE_v^f - k_B T \ln \frac{N!}{n!(N-n)!}. \quad (2b)$$

In the thermal equilibrium condition, G will be certainly minimum as related to the variation of the defect number n ,

i.e. the following condition shall be satisfied: $(\frac{\partial G}{\partial n})_T = 0$. In this case taking into account that $N \gg n$, we will have the following from (1)

$$\frac{n}{N-n} \approx \frac{n}{N} = \exp\left(-\frac{E_v^{\text{form}}}{k_B T}\right). \quad (3)$$

This means that the number of j type point defects in the volume unit n vs. the number of atoms in the volume unit N is the relative concentration C_j^{eR} of j defects. I.e. $(\frac{n}{N})$ characterizes the probability of j defect presence in the crystal.

While in equation (3), the number of atoms (points) N in the crystal volume $V = 1 \text{ cm}^3$ characterizes the density (ρ_c , cm^{-3}), then the expression for the absolute equilibrium concentration of j type point defects C_j^e will be as follows

$$C_j^e = \rho_c C_j^{eR} = \rho_c \exp\left(-\frac{E_j^f}{k_B T}\right), \quad (4a)$$

$$C = N_{\text{sites}} \exp\left(-\frac{E_j^f}{k_B T}\right), \quad (4b)$$

where N_{sites} is the number of points in which the defect may be detected.

The foregoing means that taking into account E_j^f , the defect concentration of Cu_{Zn} acceptor in ZnO (in our case) is defined using equation (4b). The equilibrium concentration of thermal defects in $\text{Zn}_{1-x}\text{Cu}_x\text{O}$ increases with the increase in temperature. The point defect concentration is defined not only by the formation temperature and energy, but also by the partial oxygen pressure.

Formation of Cu_{Zn} substitution defects in the cation position of ZnO crystalline lattice corresponds to the condition of substitution of Zn atoms similar in charge, coordination numbers, dimensions and electronic properties with Cu substitutional impurity atoms. Substitutional defects like other defects influence the properties of $\text{Zn}_{1-x}\text{Cu}_x\text{O}$ material. In particular, Cu_{Zn} defects modify the magnetic properties.

Chemical potential. Formation energy ($E_{\text{Cu}_{\text{Zn}}}^f$) of Cu_{Zn} acceptor in ZnO is defined by the relative concentration of Zn, O and Cu atoms. And the energy of zinc substitution with Cu_{Zn} acceptor is a function of chemical potentials (μ) of Zn and Cu atoms, i.e. μ_{Zn} and μ_{Cu} or $\mu(\text{Zn})$ and $\mu(\text{Cu})$. Since μ is an intensive variable like pressure p and temperature T , μ does not depend on the system weight and for the i -th component

$$\mu_i = \left(\frac{\partial G}{\partial n_i}\right)_{n_j \neq i, T, p}$$

In other words, μ_i is the Gibbs partial molar free energy ($\bar{G}_i = \mu_i$) at T , $p = \text{const}$ and constant number of moles of other j components. Therefore, for a k -component system,

$$G = \sum_{i=1}^k n_i \mu_i \text{ is true, where } n_i \text{ is the number of moles.}$$

From the free energy potentials (Helmholtz energy F , enthalpy H , internal energy U) only for Gibbs free energy, the numbers of moles of n_1, \dots, n_k components are the only extensive variables. In other words, for free energy potentials F, H and U , including also other extensive variables, when the number of moles n_i is changed, the same equation $G = \sum_{i=1}^k n_i \mu_i$ is not the case:

$$\mu_i = \left(\frac{\partial F}{\partial n_i} \right)_{n_j, T, V} = \left(\frac{\partial H}{\partial n_i} \right)_{n_j, S, p} = \left(\frac{\partial U}{\partial n_i} \right)_{n_j, V, S},$$

where V is the system volume and S is the entropy. Thus, the component's chemical potential

$$\mu_i = \left(\frac{\partial G}{\partial n_i} \right)_{n_j \neq i, T, p}$$

is defined as the energy necessary to add an atom of this component to the system.

Given that μ is the increment of Gibbs free energy G per mole (1 mol), then μ in a multicomponent system characterizes the equilibrium between components (substances). The chemical potential of a substance is a driving force for mass transfer and μ is aligned with the process progress. When the equilibrium is achieved, μ becomes equal in all coexisting phases. In the given ZnO–Cu system, to ensure formation of $\text{Zn}_{1-x}\text{Cu}_x\text{O}$ structure, for example, one Cu atom shall be added to ZnO crystal and one Zn atom shall be removed.

The formation energy of neutral Cu_{Zn} acceptor in $\text{Zn}_{1-x}\text{Cu}_x\text{O}$ super cell was calculated using the following equation

$$E_{\text{Cu}_{\text{Zn}}}^f = E(\text{ZnO}:\text{Cu}_{\text{Zn}}) - E(\text{ZnO}) + \mu(\text{Zn}) - \mu(\text{Cu}), \quad (5)$$

where $E(\text{ZnO}:\text{Cu}_{\text{Zn}})$ is the total energy of the copper-doped super cell, $E(\text{ZnO})$ is the super cell energy without Cu impurity, $\mu(\text{Zn})$ and $\mu(\text{Cu})$ are chemical potentials of Zn and Cu atoms in the ground state in gas phase (g), respectively.

Assuming $\mu(\text{Zn}^g) = 94.81$ kJ/mol and $\mu(\text{Cu}^g) = 298.31$ kJ/mol from [27] for the chemical potential, we obtain Cu_{Zn} defect formation energy using equation (5). The calculated Cu_{Zn} acceptor formation energy for the studied $\text{Zn}_{1-x}\text{Cu}_x\text{O}$ super cells is close to the results for similar $\text{Zn}_{1-x}\text{Cu}_x\text{O}$ compounds (Table 2).

Table 2. The calculated point defect formation energies in $\text{Zn}_{1-x}\text{Cu}_x\text{O}$ at absolute zero

Compound	Defect	E_{form} , eV
$\text{Zn}_{0.944}\text{Cu}_{0.056}\text{O}$	Cu_{Zn}	2.17
$\text{Zn}_{0.944}\text{Cu}_{0.056}\text{O}$	V_{Zn}	5.7
$\text{Cu}_{0.0417}\text{Zn}_{0.9583}\text{O}$	Cu_{Zn}	2.24 [12]
$\text{Cu}_{0.0278}\text{Zn}_{0.9722}\text{O}$	Cu_{Zn}	3.10 [12]

Table 3. DFT calculations of magnetic moments (M) in $\text{Zn}_{1-x}\text{Cu}_x\text{O}$ super cell

Super cell $\text{Zn}_{0.944}\text{Cu}_{0.056}\text{O}$ (Zn 3d, O 4p, Cu 3d)	Method	M, (μ_B/Cu)
$(2 \times 2 \times 1)$	LSDA + U	0.898
$(2 \times 2 \times 1)$	SGGA + U	0.998
$(3 \times 3 \times 1)$ with Zn vacancy	SGGA + U	3.0
ZnO films, 2 at.% Cu doped	Experiment at 300 K	0.15 [17]

3.5. Magnetic properties of $\text{Zn}_{1-x}\text{Cu}_x\text{O}$

The band theory of semiconductors is known to be based on a single-electron approximation and spin ordering of magnets is associated with spatial and spin correlations of electrons. It means that the latter is associated with many-electron processes. However, the use of the exchange interaction model makes it possible to assess the magnetic properties of a material in kinetic processes.

ZnO doped with metals, including Cu, at room temperature is ferromagnetic [17]. Our DFT calculations of the exchange-correlation potential in $\text{Zn}_{0.944}\text{Cu}_{0.056}\text{O}$ ($3 \times 3 \times 1$) agree with the specified potential and show that a localized magnetic moment is generated at low Cu concentrations up to 2 at%. In order to enhance the contribution of the spin magnetic moment to the magnetic moment in the calculations as mentioned above, electron-electron term exchange interaction (U) was considered.

Table 3 shows the simulation results for $\text{Zn}_{0.944}\text{Cu}_{0.056}\text{O}$ super cell containing one Zn vacancy. Vacancy incorporation (in particular, the 13-th zinc atom in the super cell) in $\text{Zn}_{0.944}\text{Cu}_{0.056}\text{O}$ matrix changes the electronic state of zinc and copper atoms. Generation of a localized magnetic moment near this zinc vacancy is a collective effect, including the electron spin as well.

The significant difference between the calculated and experimental values of μ_B (Table 3) may be probably attributable, among other things, to the magnetic anisotropy in copper-doped ferromagnetic ZnO-based materials [17,18] and to the component vapor pressures, including P_{O_2} .

Cu 3d impurity atom positions in ZnO crystal lattice and local environment of Cu 3d-atoms as well as the presence of other donors and acceptors in the samples may influence the magnetic moment magnitudes. 3d-elements are characterized by the existence in more than one charge states which depend on the local environment of these atoms. In view of the foregoing, it may be concluded that additional investigations of magnetic properties of $\text{Zn}_{1-x}\text{Cu}_x\text{O}$ are required in order to understand the causes of controversy.

In the calculated $\text{Zn}_{0.944}\text{Cu}_{0.056}\text{O}$ configuration with zinc vacancy, the electron density near Zn vacancy is changed. Zn vacancy causes the formation of dangling bonds and

the exchange interaction occurs between the localized spins of the nearest neighbors of Zn vacancy leading to ferromagnetism in $Zn_{0.944}Cu_{0.056}O$. However, the interconnected electrons of Zn^{2+} and Cu^{2+} ions of $Zn_{0.944}Cu_{0.056}O$ crystal lattice may also contribute to the magnetic moment. This means that the magnetic moment of the electron shells of $Zn_{1-x}Cu_xO$ defect atoms and molecules is composed of spin and orbital magnetic moments of electrons. Thus, the above mentioned changes in the electronic states in $Zn_{1-x}Cu_xO$ structure result in generation of a localized magnetic moment.

As shown in Table 3 for $Zn_{0.944}Cu_{0.056}O$ containing Zn vacancy, the calculated total localized magnetic moment ($0.998\mu_B$) depends on the calculation method and the electronic state of the atoms adjacent to Zn vacancy.

3.6. Charge transfer in $Zn_{1-x}Cu_xO$

The heterogenous system equilibrium condition implies that restrictions are imposed on the chemical potentials. When the equilibrium is achieved, μ becomes equal in all coexisting phases. In view of $\mu(Zn)$ and $\mu(Cu)$ in $Zn_{1-x}Cu_xO$, consider the coexistence of phases in ZnO– Cu_2O system. $T-x$ of ZnO– Cu_2O phase diagram at $P_{O_2} = 0.21$ atm [10] implies that ZnO-based Cu_2O solubility is negligible.

If $T-x$ isothermal cross-section of Zn–O–Cu system is visualized, then equilibrium conditions may be defined from it for chemical potentials of components. The upper limit of $\mu(Zn)$ is set by the free energy potential of ZnO. On the one hand, ZnO is in equilibrium with three-dimensional Zn, and on the other hand, with oxygen. The upper limit of $\mu(Cu)$ is defined by the Gibbs potential (free enthalpy) of Cu_2O , which is in equilibrium with ZnO. The lower limits of $\mu(Zn)$ and $\mu(Cu)$ comply with the chemical potentials of three-dimensional Zn and Cu components.

The chemical potential limits define the minimum dopant formation energy. This, in turn, is the maximum values for Cu impurity concentration in $Zn_{1-x}Cu_xO$. The minimum formation energy of Cu_{Zn} acceptor defect in ZnO corresponds to the condition when ZnO is in equilibrium with three-dimensional oxygen and with Cu_2O . During crystallization of ZnO-based compounds in ZnO– Cu_2O system, homogenous Cu (1–2 at.%) solutions are generated in ZnO. In view of this, lightly copper-doped $Zn_{1-x}Cu_xO$ ($x = 0, 0.01$ and 0.02) compounds were used for electrical measurements.

Direct current conduction (σ_{dc}) of ZnO samples both pure and copper-doped $Zn_{1-x}Cu_xO$ ($x = 0, 0.01$ and 0.02). The review of temperature dependences σ_{dc} of the samples has shown that in the range of 300–400 K the trend of $\sigma_{dc}(T)$ curves in Arrhenius coordinates is exponential in nature and corresponds to the semiconductor type conduction. With the increase in copper content in ZnO, sample conduction was increased and $\sigma_{dc}(1/T)$ curve slope was decreased. The conduction (E_t) activation energies

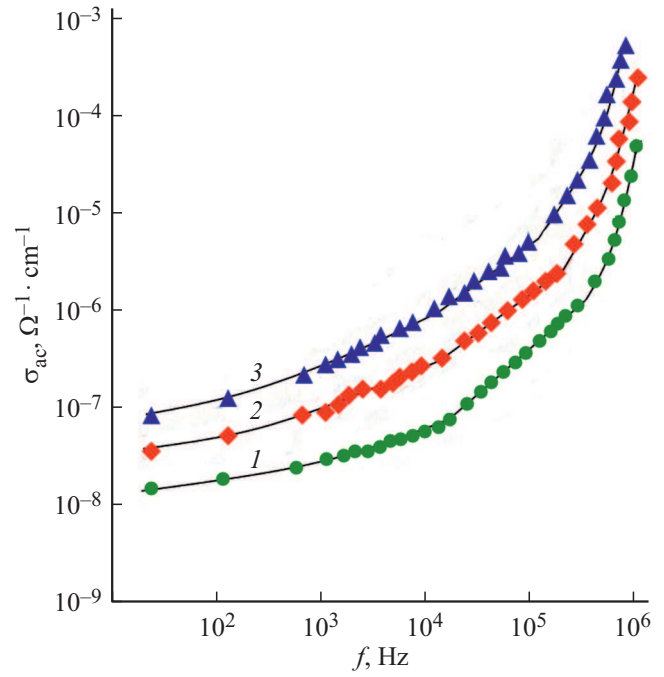


Figure 6. Frequency-dependent ac-conduction of $Zn_{1-x}Cu_xO$ samples: 1 — ZnO; 2 — $Zn_{0.99}Cu_{0.01}O$; 3 — $Zn_{0.98}Cu_{0.02}O$. $T = 300$ K.

assessed by $\sigma_{dc}(1/T)$ curve slopes for $Zn_{1-x}Cu_xO$ samples ($x = 0, 0.01$ and 0.02) are shown in Table 4.

Alternating current conduction (σ_{ac}). With the increase in copper concentration in $Zn_{1-x}Cu_xO$ samples, their σ_{ac} also was increased. Figure 6 shows the frequency dependences σ_{ac} of $Zn_{1-x}Cu_xO$ samples at room temperatures.

The specified frequency curves of $Zn_{1-x}Cu_xO$ samples consisted of three segments. A low-frequency segment in the range from 20 Hz to $1.8 \cdot 10^4$ Hz was characterized by a weak frequency dependence. In $1.8 \cdot 10^4$ – $4.3 \cdot 10^5$ Hz range, $\sigma_{ac} \sim f^{0.8}$ segment was observed, and in a higher frequency range up to 10^6 Hz, a superlinear growth of conduction took place. The obtained $\sigma_{ac} \sim f^{0.8}$ dependences in $Zn_{1-x}Cu_xO$ are indicative of charge transfer hopping among the states localized in the vicinity of the Fermi level [28,29]:

$$\sigma_{ac}(f) = \frac{\pi^3}{96} e^2 k_B T N_F^2 a^5 f \left[\ln \left(\frac{\nu_{ph}}{f} \right) \right]^4, \quad (6)$$

where e is the electron charge; k_B is the Boltzmann's constant; N_F is the density of states near the Fermi level; $a = 1/\alpha$ is the localization radius; α is the decay constant of the localized charge carrier wavefunction $\psi \sim e^{-\alpha r}$; ν_{ph} is the phonon frequency.

According to equation (6), ac-conduction depends on frequency as $f [\ln(\nu_{ph}/f)]^4$, i.e. at $f \ll \nu_{ph}$, σ_{ac} is proportional to $f^{0.8}$. Using equation (6), the Fermi-level density of states was calculated from the experimental values of $\sigma_{ac}(f)$. The calculated values of N_F for $Zn_{1-x}Cu_xO$ are listed in Table 5.

Table 4. Calculated conduction activation energies (E_t) for $Zn_{1-x}Cu_xO$ samples ($x = 0, 0.01$ and 0.02)

Compound	E_t , eV
ZnO	0.180
$Zn_{0.99}Cu_{0.01}O$	0.175
$Zn_{0.98}Cu_{0.02}O$	0.160

Table 5. Calculated density of states and energy spread of localized states near the Fermi level

Sample	N_F , $eV^{-1} \cdot cm^{-3}$	ΔE , eV
ZnO	$3.3 \cdot 10^{18}$	0.012
$Zn_{0.99}Cu_{0.01}O$	$6.7 \cdot 10^{18}$	0.006
$Zn_{0.98}Cu_{0.02}O$	$1.5 \cdot 10^{19}$	0.003

For calculations of N_F , ν_{ph} is assumed equal to 10^{12} Hz, and the localization radius is taken as $a = 30 \text{ \AA}$ like in semiconductor chalcogenide compounds [30].

According to the hopping AC conduction theory, the average hop range (R) is defined as follows

$$R = \frac{1}{2\alpha} \ln \left(\frac{\nu_{ph}}{f} \right). \quad (7)$$

R calculated using equation (7) for $Zn_{1-x}Cu_xO$ samples were equal to 230 \AA . Using R values calculated as follows

$$\tau^{-1} = \nu_{ph} \exp(-2\alpha R) \quad (8)$$

the average hopping time in $Zn_{1-x}Cu_xO$ was defined: $\tau = 4.5 \cdot 10^{-6}$ s.

Using the equation from [29]:

$$\Delta E = 3/2 \pi R^3 N_F \quad (9)$$

the energy spread of localized states near the Fermi level (ΔE) in $Zn_{1-x}Cu_xO$ was assessed. These calculated ΔE values are shown in the last column in Table 5. And using the equation

$$N_t = N_F \Delta E \quad (10)$$

the deep trap concentration in $Zn_{1-x}Cu_xO$ responsible for ac-conduction $N_t = (4-4.5) \cdot 10^{16} \text{ cm}^{-3}$ was assessed.

4. Conclusion

DFT calculations of $Zn_{1-x}Cu_xO$ wurtzite band structure (where $x = 0, 0.01$ and 0.02) based on the electron density functional made it possible to find electronic parameters of critical points in the electronic density distribution for the selected super cell compositions. Introduction of

copper into ZnO causes the change in the impurity and valence band of ZnO, and the bottom of valence band is displaced towards lower energies. After copper doping, $Zn_{1-x}Cu_xO$ band gap is reduced which decreased the energy required for electron transition from the valence band to the conduction band. It has been found that, for example, $Zn_{0.944}Cu_{0.056}O$ crystal is a direct-band crystal with band gap 3.11 eV which complies with optical and electrophysical data. The total density of electronic states in $Zn_{1-x}Cu_xO$ near the Fermi level is mainly defined by $3d$ -states of Zn ($3d^{10}4s^2$), Cu ($3d^{10}4s^1$) and by $2p$ -state of oxygen ($2s^22p^4$), and contributions associated with s -states of Zn, Cu and O have a significantly lower value. Participation of vacancy in $Zn_{1-x}Cu_xO$ structures containing 1–2 at.% Cu significantly changes the magnetic properties as well. It has been found that copper-doped ZnO obtains magnetic moment 0.898–0.998 μ_B . And the introduction of one zinc vacancy into $Zn_{1-x}Cu_xO$ super cell increases the magnetic moment up to $\sim 3 \mu_B$.

By substituting Zn in the point, Cu impurity shows strong functionality as an isoelectronic acceptor and influence the valence band. The changes in the electronic structure influence $Zn_{1-x}Cu_xO$ properties, in particular, the formed magnetic moment both during light and heavy doping and significantly reduces the band gap. This explains the cause of the property change patterns, including dielectric properties, observed in the concentration dependences. With the increase in copper concentration in $Zn_{1-x}Cu_xO$ ($x = 0, 0.01$ and 0.02), both dc- and ac-conduction was increased and the conduction activation energy was reduced from 0.180 to 0.160 eV. In $1.8 \cdot 10^4 - 4.3 \cdot 10^5$ Hz range, ac-conduction of $Zn_{1-x}Cu_xO$ was subject to $\sigma_{ac} \sim f^{0.8}$ law typical of the charge transfer hopping among the localized states near the Fermi level. The calculated parameters of the states ($N_F = 3.3 \cdot 10^{18}$, $6.7 \cdot 10^{18}$ and $1.5 \cdot 10^{19} \text{ eV}^{-1} \text{ cm}^{-3}$; $\Delta E = 0.012$, 0.006 and 0.003 eV) localized in $Zn_{1-x}Cu_xO$ ($x = 0, 0.01$ and 0.02) band gap are consistently changed with the growth of copper concentration in the samples. Thus, copper introduction into zinc oxide makes it possible to control its dielectric properties which is important for VVR materials.

Funding

The study has been supported by the Science Development Foundation under the President of the Republic of Azerbaijan (EIF) (grant No. EIF-BGM-3-BRFTF-2+/2017-15/05/1-M-13) and the Russian Foundation for Basic Research (RFBR) (project No. Az_a2018).

Conflict of interest

The authors declare that they have no conflict of interest.

References

- [1] J. He. Metal Oxide Varistors (From Microstructure to Macro-Characteristics). Wiley–VCH Verlag GmbH & Co. KGaA (2019). 465 p. ISBN: 9783527333820
- [2] A. Janotti, C.G. Van de Walle. Rep. Prog. Phys. **72**, 12, 126501 (2009). <http://dx.doi.org/10.1088/0034-4885/72/12/126501>
- [3] H. Morkoç, Ü. Özgür. Zinc Oxide. Fundamentals, Materials and Device Technology. Wiley–VCH Verlag GmbH & Co. KGaA (2009). 477 p. ISBN: 9783527408139
- [4] E.C. Lee, K.J. Chang. Phys. Rev. B **70**, 11, 115210 (2004). <http://dx.doi.org/10.1103/physrevb.70.115210>
- [5] L. Chow, O. Lupan, G. Chai, H. Khallaf, L.K. Ono, B. Roldan Cuenya, I.M. Tiginyanu, V.V. Ursaki, V. Sontea, A. Schulte. Sens Actuators A **189**, 399 (2013). <http://dx.doi.org/10.1016/j.sna.2012.09.006>
- [6] B. Kulyk, B. Sahraoui, V. Figa, B. Turko, V. Rudyk, A. Kapustiansky. J. Alloys Compd. **481**, 819 (2009). <http://dx.doi.org/10.1016/j.jallcom.2009.03.117>
- [7] Y. Yan, M.M. Al-Jassim, S.H. Wei. Appl. Phys. Lett. **89**, 181912 (2006). <http://dx.doi.org/10.1063/1.2378404>
- [8] L. Chow, O. Lupan, G. Chai, H. Khallaf, L.K. Ono, B. Roldan Cuenya, I.M. Tiginyanu, V.V. Ursaki, V. Sontea, A. Schulte. Sensors Actuators A **189**, 399 (2013). <http://dx.doi.org/10.1016/j.sna.2012.09.006>
- [9] S.A. Ahmed. J. Mater. Sci. Mater. Electron. **28**, 3733 (2017). <http://dx.doi.org/10.1007/s10854-016-5981-4>
- [10] X. Longgong, L. Zhihong, Taskinen, P. Antero. Ceram. Int. **42**, 4, 5418 (2016). <http://dx.doi.org/10.1016/j.ceramint.2015.12.082>
- [11] C.G. Van de Walle, D.B. Laks, G.F. Neumark, S.T. Pantelides. Phys. Rev. B: Condens. Matter. **47**, 15, 9425 (1993). <http://dx.doi.org/10.1103/physrevb.47.9425>
- [12] Z. Ma, F. Ren, X. Ming, Y. Long, A.A. Volinsky. Mater. **12**, 196 (2019). <http://dx.doi.org/10.3390/ma12010196>
- [13] M.F. Manzoor, E. Ahmad, M. Ullah, A.M. Rana, A.S. Malik, M. Farooq, I. Ahmad, M. Hasnain, Z.A. Shah, W.Q. Khan, U. Mehtab. Acta Phys. Pol. A **135**, 3, 458 (2019). <http://dx.doi.org/10.12693/APhysPolA.135.458>
- [14] X. Chuanhui, W. Feng, H. Chunlian. J. Alloys Compd. **589**, 604 (2014). <http://dx.doi.org/10.1016/j.jallcom.2013.11.066>
- [15] G.J. Chen, S.R. Jian, J.Y. Juang. Coatings **8**, 266 (2018). <http://dx.doi.org/10.3390/coatings8080266>
- [16] N.M. Alatawi, L. Ben Saad, L. Soltane, A. Moulahi, I. Mjejri, F. Sediri. Polyhedron **197**, 115022 (2021). <https://doi.org/10.1016/j.poly.2021.115022>
- [17] F.Y. Ran, M. Tanemura, Y. Hayashi, T. Hihara. J. Cryst. Growth **311**, 17, 4270 (2009). <http://dx.doi.org/10.1016/j.jcrysgro.2009.07.008>
- [18] T.S. Heng, S.P. Lau, S.F. Yu, H.Y. Yang, L. Wang, M. Tanemura, J.S. Chen. Appl. Phys. Lett. **903**, 032509 (2007). <http://dx.doi.org/10.1063/1.2433028>
- [19] C. Lausecker, B. Salem, X. Baillin, O. Chaix-Pluchery, H. Roussel, S. Labau, B. Pelissier, E. Appert, V. Consonni. Inorg. Chem., Am. Chem. Soc. **60**, 3, 1612 (2021). [10.1021/acs.inorgchem.0c03086](https://doi.org/10.1021/acs.inorgchem.0c03086) <https://doi.org/10.1021/acs.inorgchem.0c03086>
- [20] M. Willander. Zinc Oxide Nanostructures: Advances and Applications. CRC Press (2014). 232 p. ISBN: 9789814411349
- [21] M.M. Asadov, S.N. Mustafaeva, S.S. Guseinova, V.F. Lukichev, D.B. Tagiev. Phys. Solid State **63**, 5, 797 (2021). <https://doi.org/10.1134/S1063783421050036>
- [22] M.M. Asadov, S.N. Mustafaeva, S.S. Guseinova, V.F. Lukichev. Phys. Solid State **62**, 11, 2224 (2020). <https://doi.org/10.1134/S1063783420110037>
- [23] J. Hubbard. Proc. Roy. Soc. London A **276**, 238 (1963). <https://doi.org/10.1098/rspa.1963.0204>
- [24] S.N. Mustafaeva, M.M. Asadov, A.A. Ismailov. Phys. Solid State **51**, 11, 2269 (2009).
- [25] C.G. Van de Walle. Physica B **308–310**, 899 (2001).
- [26] Ü. Özgür, Y.I. Alivov, C. Liu, A. Teke, M.A. Reshchikov, S. Doğan, V. Avrutin, C.J. Cho, H.A. Morkoç. J. Appl. Phys. **98**, 4, 041301-0 (2005). <https://doi.org/10.1063/1.1992666>
- [27] G. Job, R. Rüffler. Physikalische Chemie. Studienbücher Chemie. Springer Fachmedien Wiesbaden GmbH, ein Teil von Springer Nature, 2021. ISBN: 978-3-658-32935-8
- [28] M. Pollak. Phil. Mag. **23**, 519 (1971). <https://doi.org/10.1080/14786437108216402>
- [29] N.F. Mott, E.A. Davis. Electronic Processes in Non-Crystalline Materials. OUP Oxford (2012). 590 p. ISBN: 9780199645336.
- [30] S.N. Mustafaeva, M.M. Asadov, S.S. Guseinova, A.I. Dzhabarov, V.F. Lukichev. Phys. Solid State **64**, 4, 423 (2022).